THE GENERATION AND OPTICAL RESPONSE OF NANOCLUSTERS

L.H. Kidder, C.A. Fancher, T.P. Lippa, H.W. Sarkas, J.V. Coe, and K.H. Bowen

Department of Chemistry, Johns Hopkins University

Baltimore, MD 21218, USA

RECENT PUBLICATIONS, SUBMITTALS, AND PRESENTATIONS:

Sarkas, H.W., Arnold, S.T., Hendricks, J.H., Slager, V.L., and Bowen, K.H., "Characterization of the $X^2\Sigma^+$ State of $^7Li_2^-$ via Negative Ion Photoelectron Spectroscopy" Z. Phys. D **29**, 209, 1994.

Arnold, S.T., Hendricks, J.H., and Bowen, K.H., "Photoelectron Spectroscopy of Solvated Anion Clusters," in *Reaction Dynamics in Clusters and Condensed Phases*, ed. J. Jortner, Kluwer Academic Publishers, Amsterdam, p 37, 1994.

Desfrancois, C., Baillon, B., and Schermann, J.P., Arnold, S.T., Hendricks, J.H., and Bowen, K.H., "Prediction and Observation of a New Ground State, Dipole-Bound Dimer Anion: The Mixed Water/Ammonia System," Phys. Rev. Lett. **72**, 48, 1994.

Sarkas, H.W., Hendricks, J.H., Arnold, S.T., and Bowen K.H., "Photoelectron Spectroscopy of Lithium Hydride Anion," J. Chem. Phys. **100**, 1, 1994.

To be Published in Proceedings of the 1994 Scientific Conference on Obscuration and Aerosol Research, ed. J. Rhodes (US Army Chemical Development and Engineering Center, June 1994) US Army Report No. CRDEC-SP-)

Sarkas, H.W., Hendricks, J.H., Arnold, S.T., Slager, V.L., and Bowen K.H., "Measurement of the $X^2\Sigma^+$ - $A^2\Pi$ Splitting in CsO via Photoelectron Spectroscopy of CsO^-," J. Chem. Phys. **100**, 3358, 1994.

Sarkas, H.W., Kidder, L.H., and Bowen, K.H., "Photoelectron Spectroscopy of Color Centers in Negatively Charged Cesium Iodide Nanocrystals," J. Chem. Phys., in press.

Sarkas, H.W., Arnold, S.T., Hendricks, J.H., Kidder, L.H., Jones, C.A., and Bowen, K.H., "An Investigation of Catalytic Activity in Mixed Metal Oxide Nanophase Materials," Z. Phys. D **26**, 46, 1993.

ABSTRACT

We report on our continuing use of an inert gas condensation based ion source to generate and characterize (1) beams of nanocluster ions, and (2) neutral nanopowders. We are able to make small, nanometer sized clusters of many different materials using this source. It employs a novel combination of the inert gas condensation method for creating clusters, with techniques for injecting electrons directly into expanding jets. The hallmark of the source is its ability to produce, from a variety of materials, intense beams of ions (positive and negative), and bulk quantities of nanophase powders. This source makes nearly space charge limited beams of negative cluster ions, and has generated bulk samples of dispersable nanophase powders. We have explored the electronic and optical response of nanocluster anions using two spectroscopic techniques. Also, bulk samples of nanophase powders produced by the source have been characterized.

Introduction

Nanoclusters possess potentially useful attributes, such as high surface-to-volume ratios, a high degree of geometrical surface defects, and unique electronic structures. Because of the unique properties of, and interactions between nanoclusters, materials assembled from them differ from conventional materials. Therefore, nanoclusters can be used as building blocks to design new materials exhibiting unique or improved electronic, magnetic, optical, mechanical, and chemical properties. We report on our continuing use of an inert gas condensation based ion source[1] (hereby referred to as the Smoke-Ion Source) to generate and characterize: (1) beams of nanocluster ions, and (2) neutral nanopowders. This source has made close to space charge limited beams of some cluster ions,[2] and generated bulk samples of nanophase powders.[3]

The Smoke-Ion Source is a novel combination of the inert gas condensation method for generating clusters,[4] with techniques for injecting electrons directly into expanding jets.[5] The hallmark of the source is its ability to produce, from a variety of materials, intense beams of ions (positive and negative), and bulk quantities of nanophase powders. The size, composition, and distribution of the cluster ion beam is characterized by coupling the source to a mass selected beam line. These characteristics (cluster size, composition, and distribution) can be monitored during ion beam production, and changed by varying ion source conditions. Since nanophase powders are produced simultaneously with the ion beam, their characteristics correlate with the ion beam, and also change with ion source conditions. Consequently, because the source simultaneously produces ions beams and nanophase powders, one has the unique ability to monitor and change the cluster size and distributions of both the cluster ions and nanophase powders as they are being made .

Experimental

The Smoke-Ion Source consists of a cooling jacket which can be maintained at constant temperatures between 77 K and 285 K, a condensation cell containing inert gas (usually

between 1 and 10 torr of helium), a small sampling aperture that couples the source to a mass spectrometer, and a heat shielded sample holder where the material of interest is evaporated (see figure 1). The material of interest is placed in an appropriate crucible, and resistive heating is used to vaporize the sample, although other methods such as sputtering or laser vaporization could be used. The temperature of the bath gas in the condensation cell is controlled by the cooling jacket, which can be held at a variety of temperatures using liquid nitrogen, dry ice, or other coolants. When the hot vapor from the sample encounters the cold bath gas, the vapor supersaturates and nucleates, forming nanometer sized clusters. Colder bath gas temperatures lead to higher supersaturation ratios, resulting in the formation of larger clusters. Thus changing the temperature of the cooling jacket changes the size of the clusters produced in the condensation cell.

When the source is coupled to a mass spectrometer beam line, it is housed inside of a vacuum chamber that operates at 10^{-5} torr when under load. A sampling aperture (usually 1-2mm) is mounted on the front of the source. The pressure difference between the condensation cell and vacuum chamber results in a helium flow which entrains some of the nanoclusters, transporting them into the vacuum chamber via a weak supersonic expansion. The corresponding nanopowders are formed from clusters that remain within the condensation cell, and collect on the cold walls of the source. The transported clusters are ionized using a negatively biased filament located just outside the source aperture, which serves as a thermionic cathode, creating a discharge in the environment of the weakly expanding jet. The resulting plasma is confined by an axial magnetic field created by six cylindrical rare earth magnets. The cluster ions are then extracted and transported along the beam line, mass selected by a Wien filter, and detected with a Faraday cup. The Wien filter acts to "purify" the ion beam relative to cluster size, enabling the size, distribution, and composition of the cluster ions produced to be monitored.

When the sampling aperture on the front of the source is blanked off, the Smoke-Ion Source is decoupled from the beam line, and can be used exclusively to generate bulk nanopowders. In

this configuration, it is not possible to monitor the size and distribution of the nanopowders via mass spectroscopic characterization of the corresponding ion beam, but greater quantities of the powders can be produced.

Production and Mass Spectral Characterization of Nanocluster Ions

The Smoke-Ion Source is capable of producing beams of both negative and positive ions. The spectra in figure 2 show lead cluster cations and anions made from this source. The cluster distributions for large clusters are very similar, both starting with ~40 lead atoms per cluster ion, peaking at 200 lead atoms per cluster ion, and diminishing with ~400 lead atoms per cluster ion. The similarity between the two indicates that the ionic distributions are comparable to the neutral distribution within the condensation cell. This is further evidence that mass spectrometric information obtained for nanocluster ion beams can be used to monitor the size and distribution of corresponding neutral nanopowders.

The Smoke-Ion Source is also capable of producing beams of both large and small cluster ions. Mass spectra showing two different size distributions of lead clusters ions are shown in figure 3. To access the heavy clusters mass spectrometrically, the resolution of the Wien filter must be turned down, leading to a situation in which individual lead cluster ions are no longer resolved. The cluster ion distributions in figure 3 were produced under two different source conditions. This is an example of the information that can be obtained by coupling the source to a beam line containing a mass filter. Changes is source conditions can be directly correlated to changes in cluster size and distribution.

Nanocluster ions of a wide variety of materials have been produced using the Smoke-Ion Source. Following is a partial list of materials from which nanocluster ions have been made: vanadium, tin, sodium, germanium, aluminum, cesium iodide, copper, copper oxide, silver, and magnesium (see figures 4-12.)

The sizes of the nanoclusters made in this source are smaller than is easily accessible using many other techniques. Also, although not monodispersed, the narrowness of the size

distribution for these cluster anions is quite good. The narrowest size distribution made was for copper oxide cluster anions, shown in figure 9. The FWHM size distribution was 0.2 nm wide, and the overall distribution only spread over 0.5 nm. Copper and silver nanocluster anions give typical FWHM size distributions, of 0.4 and 0.3 nm wide, respectively (see figures 10 and 11.) Magnesium gave one of the broadest distributions, with a FWHM of 0.8 nm wide (see figure 12.)

Electronic and Optical Response of Nanocluster Anions

Beyond the mass spectral characterization of cluster ion sizes and distributions, we have also explored the electronic and optical response of nanocluster anions using two spectroscopic techniques. The electronic properties of cesium iodide nanocluster anions were probed using the technique of negative ion photoelectron spectroscopy.[6] The photoelectron spectra were collected by crossing the mass selected cluster anion beam of interest with the 2.54 eV line of an argon ion laser. Electrons bound with less than the photon energy of 2.54 eV were detached and analyzed for kinetic energy. The binding energy of the detached electrons is the quantity of interest, and it is related to the electron kinetic energy by:

$$\text{Electron Kinetic Energy} = \text{Photon Energy} - \text{Electron Binding Energy}$$

The spectra are collected as electron counts vs. electron binding energy. For cesium iodide nanocluster anions, we have taken the photoelectron spectra of CsI nanocluster anions with between 13-165 CsI units per cluster anion (figure 13).

These photoelectron spectra are similar to each other, each consisting of a single feature which shifts to successively higher electron binding energies with increasing cluster size. The low binding energy onset of the feature in each spectrum is the photodetachment threshold energy for that given cluster anion. Initially, the threshold values rise rapidly with increasing cluster size and then appear to reach an asymptotic limit. In order to understand the physical

meaning of this size dependent evolution of the threshold energies, we turn to a classical dielectric model:

$$\varepsilon_{Th}(n) = \varepsilon_{Th}(\infty) - KR^{-1}$$

ε_{Th} **(n)** corresponds to the photodetachment threshold for the cluster, n

ε_{Th} (∞) corresponds to the photoelectric threshold in bulk cesium iodide

K is a constant containing the static dielectric constant of bulk cesium iodide

n is the number of CsI units

This model predicts that cluster threshold binding energies, $\varepsilon_{Th}(n)$, will increase linearly toward their corresponding bulk energy, $\varepsilon_{Th}(\infty)$ when plotted versus the inverse of the cluster radius. Figure 14 shows a plot of the threshold energies vs $n^{-1/3}$, which is proportional to the inverse cluster radius. Plotting the data this way makes the size-dependent behavior of the threshold energies more understandable, as the intercept of this plot represents the photoelectric threshold energy at infinite cluster size, i.e. the bulk photoelectric threshold. The plot gives a straight line that extrapolates to 2.2 eV. By correlating this extrapolated value with a known bulk photoelectric value, information is gained about how the excess electrons in these nanocrystals are bound. The photoelectric threshold measured for F-centers in bulk cesium iodide samples at 300K is 2.2 eV, which is in excellent agreement to the extrapolated value. This implies that the mechanism of electron localization in these gas-phase nanocrystals is analogous to F-centers in extended alkali halide crystals. These species are thus identified as CsI nanocrystals containing single excess electrons in embryonic F-centers, which mature with increasing cluster size toward being defect centers in bulk crystalline cesium iodide.

We also took PES of CsI nanoclusters at hotter source conditions, and saw an additional low electron binding energy feature. In figure 15, the spectra on the left are the lower temperature spectra, shown for comparison next to the hotter source condition spectra on the right. The new feature shifts together with the original feature to successively higher binding energies with increasing cluster size. The appearance of this feature indicates that a new

mechanism of excess electron binding is occurring at hotter source conditions. In order to understand the cluster size dependence of the threshold energies for these low electron binding energy features, a plot of them vs $n^{-1/3}$ was made and is shown in figure 16. The slope of this line is similar to that for the F-center cluster anions, but extrapolates to a bulk value of 1.4 eV. This feature is due to a different mechanism of excess electron binding. The extrapolated value of 1.4 eV is consistent with the photoelectric threshold expected for F'-centers (two excess electrons in a single defect site) in bulk CsI. We therefore assign this feature to be CsI nanocrystals containing excess electrons in embryonic F'-centers. Using negative ion photoelectron spectroscopy of size selected clusters, we have been able to monitor the behavior of excess electron localization in negatively charged cesium iodide nanocrystals, and elucidate the size dependent evolution of embryonic F-centers and F'-centers is these nanocrystals.

Presently, we are involved in studying the optical response of small sodium cluster anions. Recently, theoretical interest has turned toward collective oscillations in metal spheres so small that the bulk dielectric constant is no longer applicable. Knight's group at Berkeley experimentally verified the existence of these resonances in small metal clusters, when they studied the optical response of small (2- 40 atoms per cluster) neutral sodium clusters.[7] They used the jellium shell model, in which the valence electrons move freely in a smeared-out positive potential (jellium background) to predict cluster geometries. They then correlated the shape of the resonances, one or multiple peaks, with the predicted cluster geometries, spherical or ellipsoidal. They observed a correlation between the cluster geometries predicted using the shell model, and the shapes of their optical response resonances.

These initial investigations sparked interest in these resonances, and experiments have been performed on large and small alkali metal cluster neutrals and cations.[8] To date though, little has been done to study small cluster anions.[9] Higher resolution studies on alkali cations show fine structure that can't be explained through the simple shell model, and there is much debate about how to best describe the nature of this classical bulk resonance when it is reduced to a quantum level. Various theoretical approaches have been put forth to better describe these

resonances, from the *ab initio* calculations of Bonacic-Koutecky, to self consistent jellium calculations of Ekardt.[10-12] Yannouleas in particular has developed a theoretical framework to describe the fine structure of the resonances for large and small, negative, positive, and neutral clusters.[13] He describes the fine structure as being due to coupling between collective dipole oscillations and single particle levels. While the observed effect is predicted to be relatively small in neutral and cationic clusters, it should be prominent for small anionic alkali clusters. Thus the optical response of small alkali cluster anions provides an important test of Yannouleas' model. We have recorded preliminary data pertaining to these resonances in both Na_7^-, an eight electron system, and Na_3^-, a four electron system, and are now in the process of obtaining the complete optical response spectra for these clusters.

Production and Characterization of Nanopowders

The Smoke-Ion Source produces nanopowders both when it is coupled to a mass spectrometer beam line, and also when the sampling aperture is blanked off. The source generates bulk quantities of powders possessing novel properties, that are easily dispersible, and might have interesting capabilities in obscuration. When the Smoke-Ion Source is coupled to the mass spectrometer beam line, the size, composition and distribution of the nanocluster ions can be monitored, and nanopowder samples can be simultaneously produced. For example, a bulk sample of chromium nanopowder was collected from the source after a mass spectrometric run. The sample was analyzed using TEM, and found to be comprised of nanocystals between 5 - 50 nm.

Also, a bulk sample of nanophase lithium magnesium oxide powder was produced by the Smoke-Ion Source when it was decoupled from the mass selected beam line.[3] Conventional bulk Li-MgO is used in the oxidative conversion of methane to higher hydrocarbons. The powder sample produced in the source showed threshold catalytic activity at ~200 C below the temperature at which conventional Li-MgO catalysts exhibit threshold activity. At higher

temperatures, the same nanophase composition showed substantially enhanced activities and somewhat improved hydrocarbon selectivities over conventional Li-MgO catalysts.

Summary

In summary, the Smoke-Ion Source can make small, nanometer sized clusters of many different materials. The clusters can be ionized and transported through a mass spectrometer beam line, and characterized as to their size, distribution, and composition. But the source also produces bulk quantities of nanopowders, either simultaneously with the production of the ion beam, or separately if the source is decoupled from the beam line. As evidenced by our completed work with $(CsI)_n^-$ and our ongoing work with sodium cluster anions, we can characterize the optical and electronic response properties of nanocluster anions. We can also make dispersible samples of the neutral nanopowders, and characterize them using a variety of methods.

This work has been sponsored partially by the National Science Foundation under grant CHE-9007445, and partially by ARCO Chemical Co.

References

1. K.M. McHugh, H.W. Sarkas, J.G. Eaton, C.R. Westgate, and K.H. Bowen, Z. Phys D. 12, 3 (1989).

2. H.W. Sarkas, L.H. Kidder, J.G. Eaton, N.G. Wimer, K.M. McHugh, and K.H. Bowen, in *Proceedings of the 1990 Scientific Conference on Obscuration and Aerosol Research*, edited by E.H. Engquist and D.A. Clark, (Commander U.S. Army Chemical Development and Engineering Center, June 1991) U.S. Army Report, No. CRDEC-SP-036, pp. 143-

161; H.W. Sarkas, L.H. Kidder, J.G. Eaton, K.M. McHugh, and K.H. Bowen, Mat. Res. Soc. Symp. Proc. 206 277 (1991).

3. H.W. Sarkas, S.T. Arnold, J.H. Hendricks, L.H. Kidder, C.A. Jones, and K.H. Bowen, Z. Phys. D-Atoms Molecules and Clusters, 26, 46 (1993).

4. T.P. Martin, J. Chem. Phys. 81, 4426 (1984); J. Muhlback, P. Pfau, K. Sattler, E. Rechnagel, Z. Phys. B 47, 233 (1982).

5. H. Haberland, H.G. Schindler, and D.R. Worsnop, Ber. Bunsenges. Phys. Chem. 88, 270 (1984); J.V. Coe, J.T. Snodgrass, C.B. Freidhoff, K.M. McHugh, and K.H. Bowen, J. Chem. Phys. 84, 618 (1986); M.L. Alexander, M.A. Johnson, N.E. Levinger, and W.C. Lineberger, Phys. Rev. Lett. 57, 976 (1986).

6. H.W. Sarkas, L.H. Kidder, and K.H. Bowen, J. Chem. Phys, submitted.

7. W.A. deHeer, K. Selby, V. Kresin, J. Masui, M. Vollmer, A. Chatelain, W.D. Knight, Phys. Rev. Lett 59, 1805 (1987); K. Selby, V. Kresin, J. Masui, M. Vollmer, W.A. deHeer, A. Scheidemann, and W.D. Knight, Phys. Rev. B 43, 4565 (1991).

8. H. Fallgren and T.P. Martin, Chem. Phys. Lett. 168, 233 (1990); N.D. Bhaskar, in *Physics and Chemistry of Finite Systems: From Clusters to Crystals*, edited by P. Jena, S.N. Khanna, and B.K. Rao (Kluwer Academic, Dordrecht, 1992) NATO ASI Series, Vol. 1, pp. 374; Th. Reiners, W. Orlik, Ch. Ellert, M. Schmidt, and H. Haberland, Chem. Phys. Lett. 215, 357 (1993); C. R. C. Wang, S. Pollack, D. Cameron, and M.M. Kappes, J. Chem. Phys. 93, 3787 (1990); C. Brechignac, Ph. Cahuzac, F. Carlier, and J. Leygnier, Chem. Phys. Lett. 164, 433 (1989).

9. Th. Reiners and H. Haberland, Phys. Rev. Lett, to be published; J. Tiggesbaumker, L. Koller, H.O. Lutz, and K.H. Meiwes-Broer, in *Nuclear Physics Concepts in the Study of Atomic Cluster Physics*, edited by H.O. Lutz (Springer-Verlag, Berlin, 1992) Lecture Notes in Physics Series, No. 404, pp. 247.

10. V. Bonacic-Koutecky, P. Fantucci, and J. Koutecky, J. Chem. Phys. 93, 3802 (1990).

11. W. Ekardt, Phys. Rev. B 31, 6360 (1985); W. Ekardt and Z. Penzar, Phys. Rev. B 43, 1322 (1991)

12. V. Kresin, Physics Reports 220, 3 (1992); V. Kresin, Phys. Rev. B 42, 3247 (1990); V. Kresin, Phys. Lett. A 133, 89 (1988).

13. C. Yannouleas and E. Vigezzi, and R.A. Broglia, Phys. Rev. B 47, 9849 (1993); C. Yannouleas, Chem. Phys. Lett. 193, 587 (1992); C. Yannouleas and R.A. Broglia, Phys. Rev. A 44, 5793 (1991).

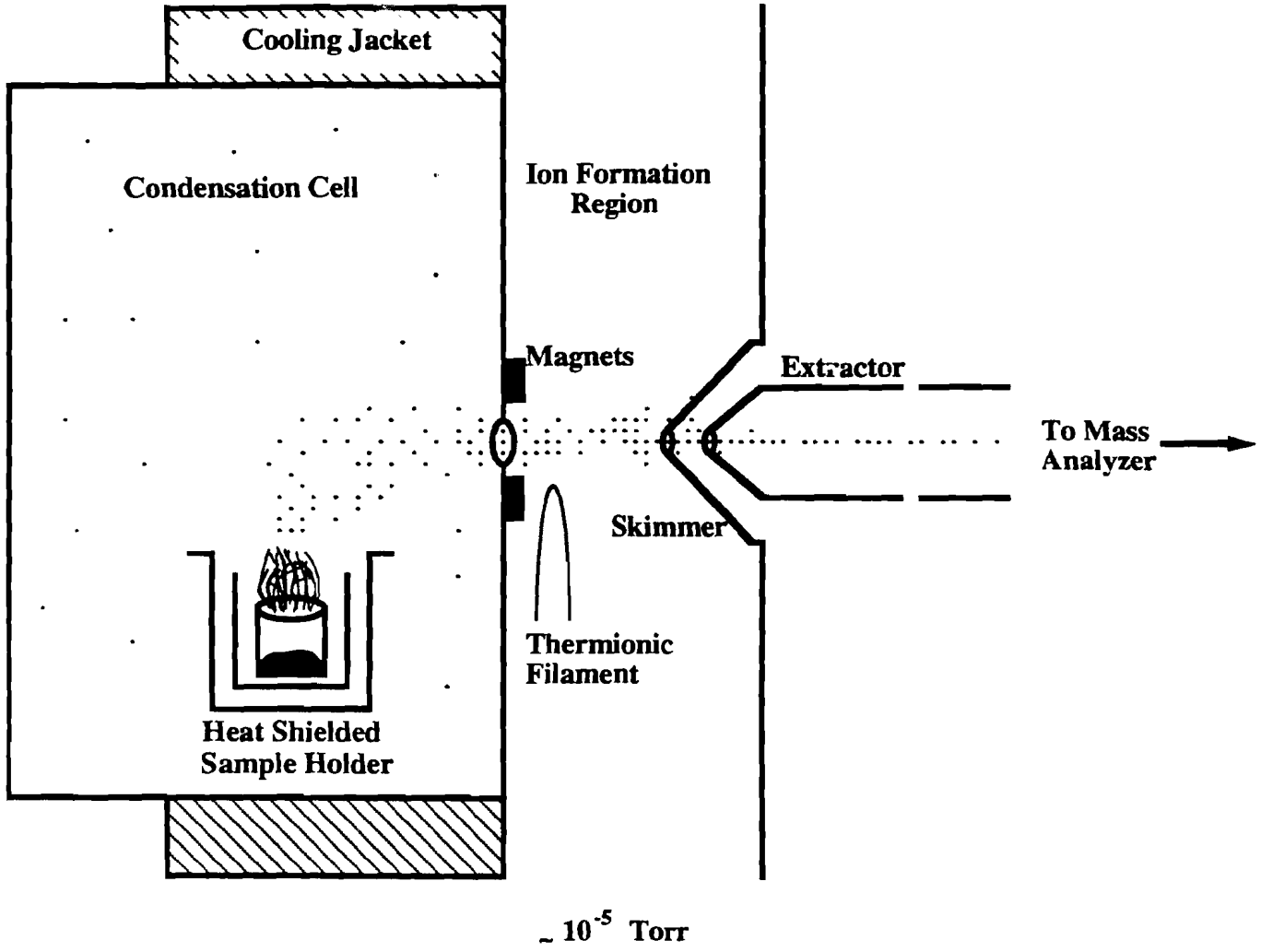

Figure 1: Inert Gas Condensation Cluster Ion Source Coupled to Mass Spectrometer

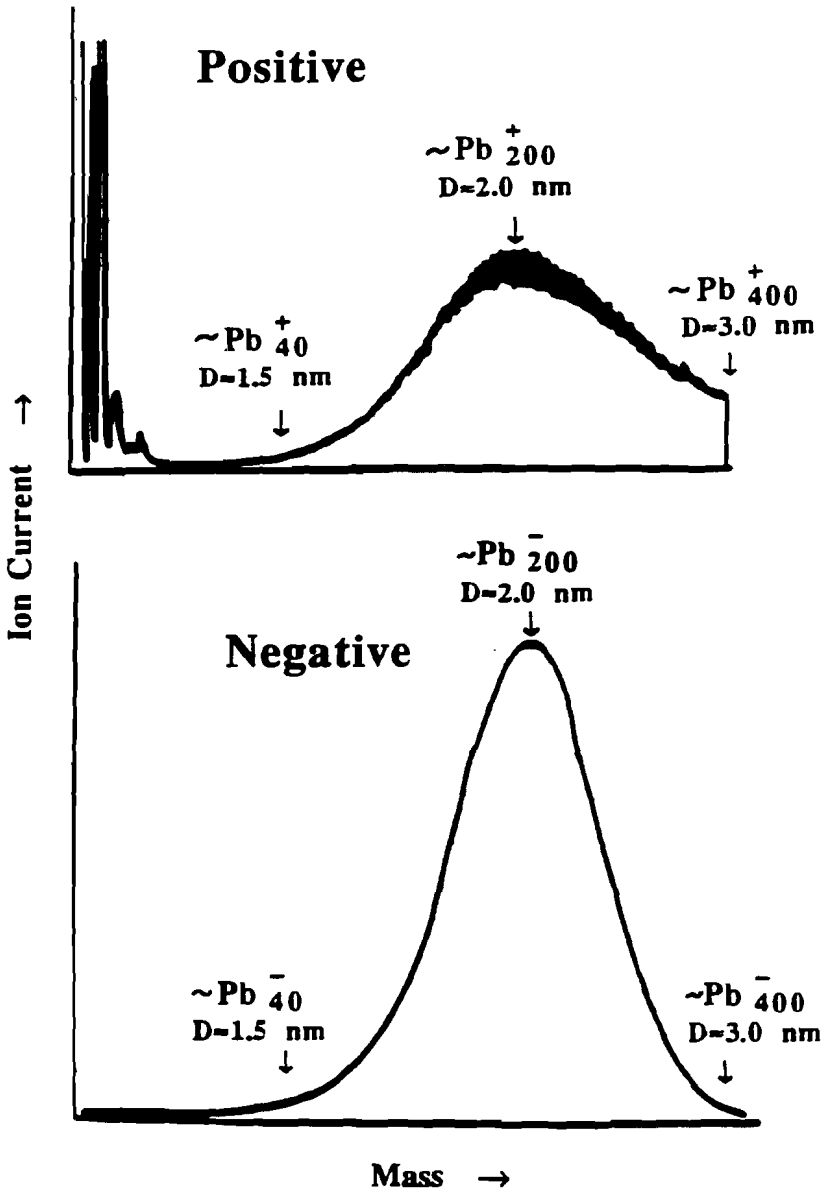

Figure 2: Mass Spectra of Negative and Positive Lead Cluster Ions

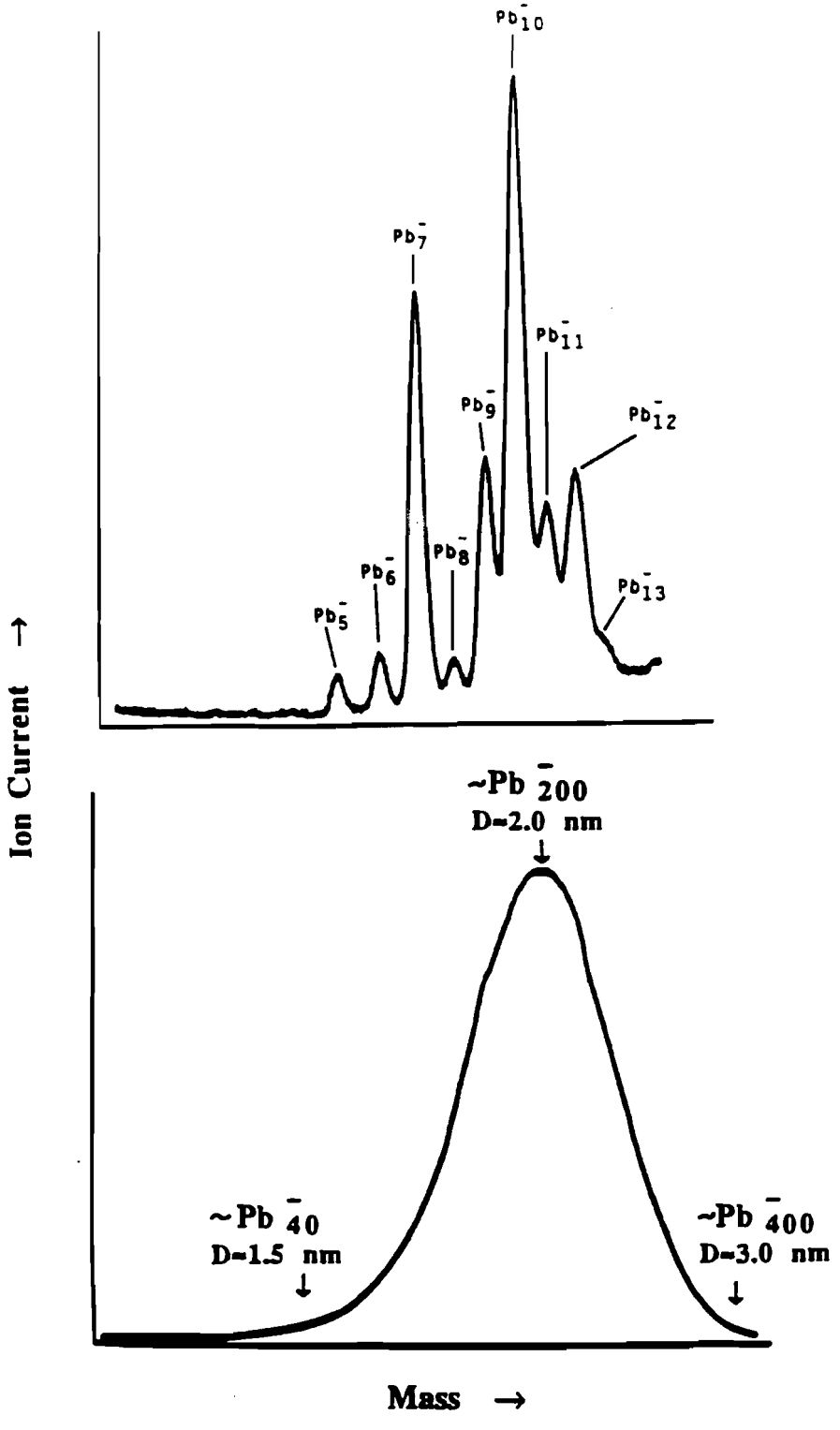

Figure 3: Mass Spectra of Small and Large Lead Cluster Anions

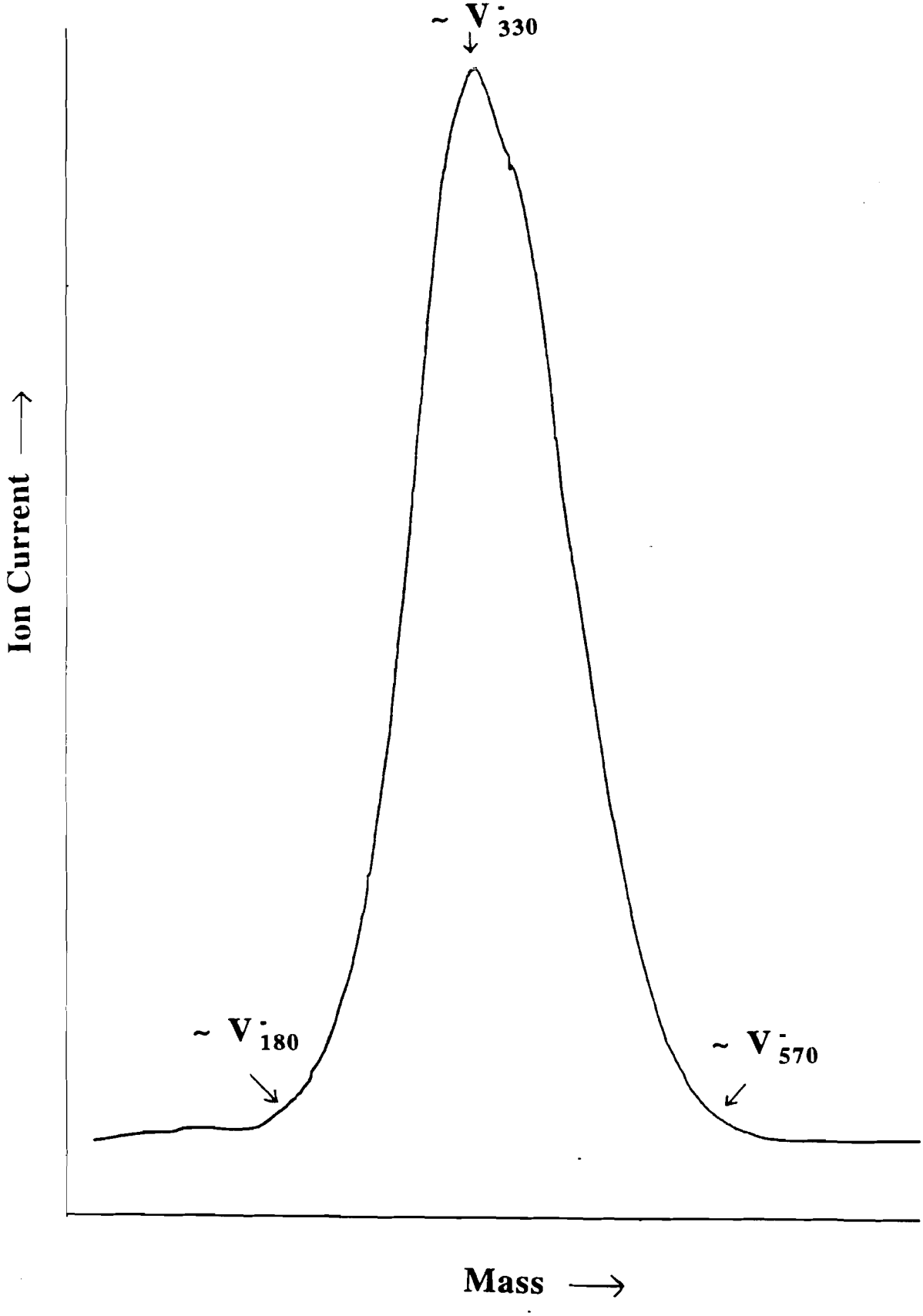

Figure 4: Mass Spectrum of Vanadium Cluster Anions

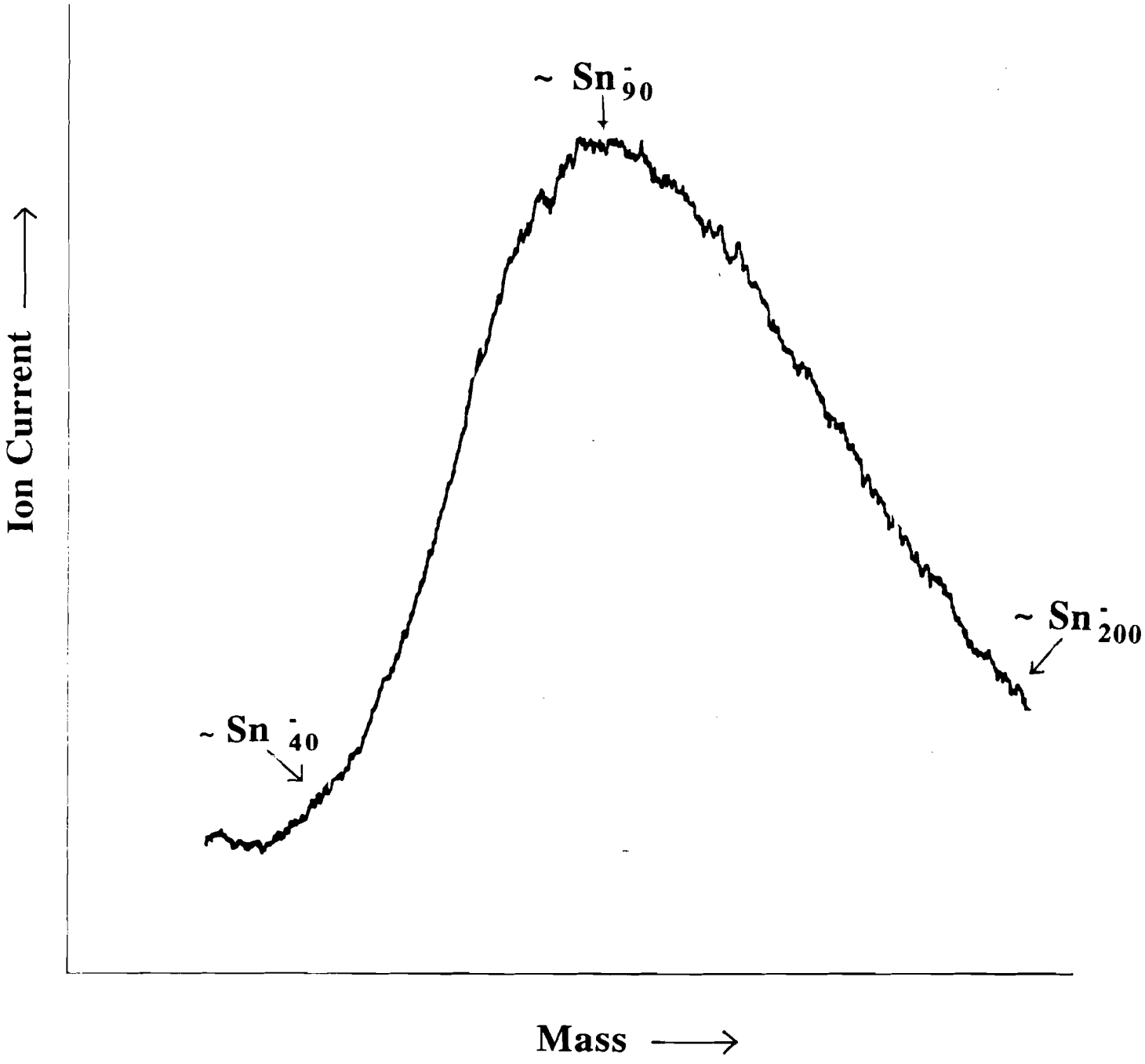

Figure 5: Mass Spectrum of Tin Cluster Anions

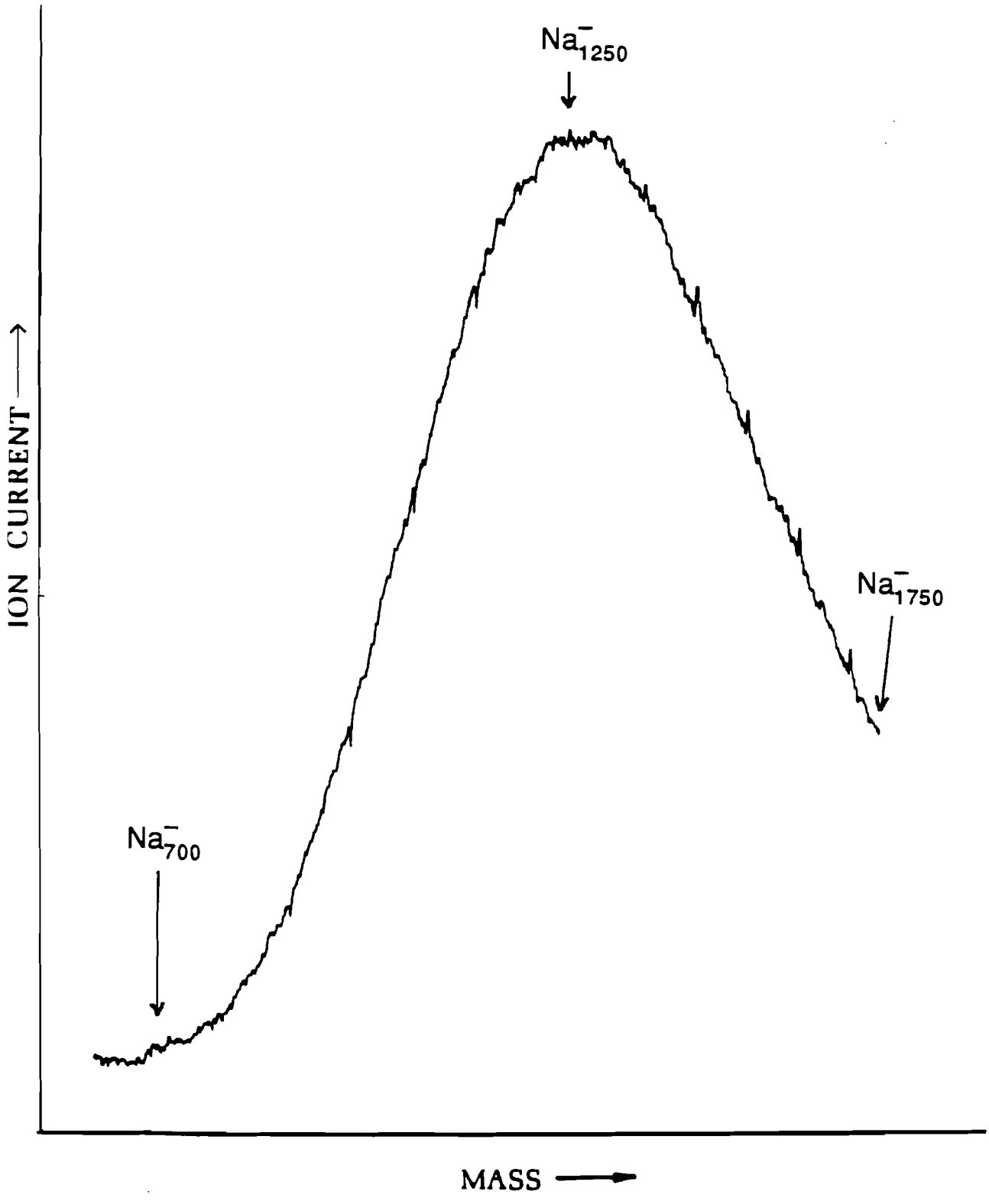

Figure 6: Mass Spectrum of Sodium Cluster Anions

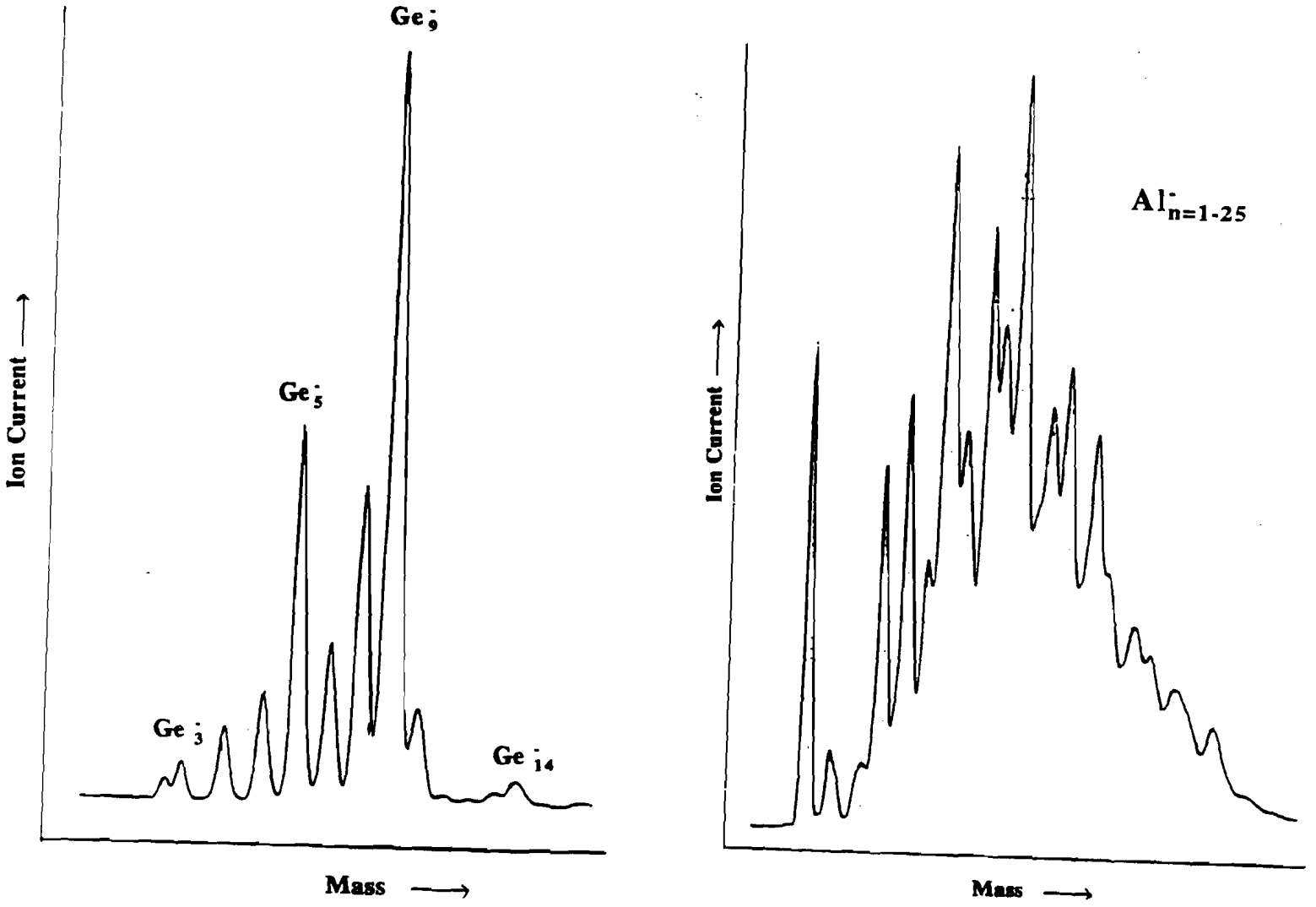

Figure 7: Mass Spectra of Small Germanium and Aluminum Cluster Anions

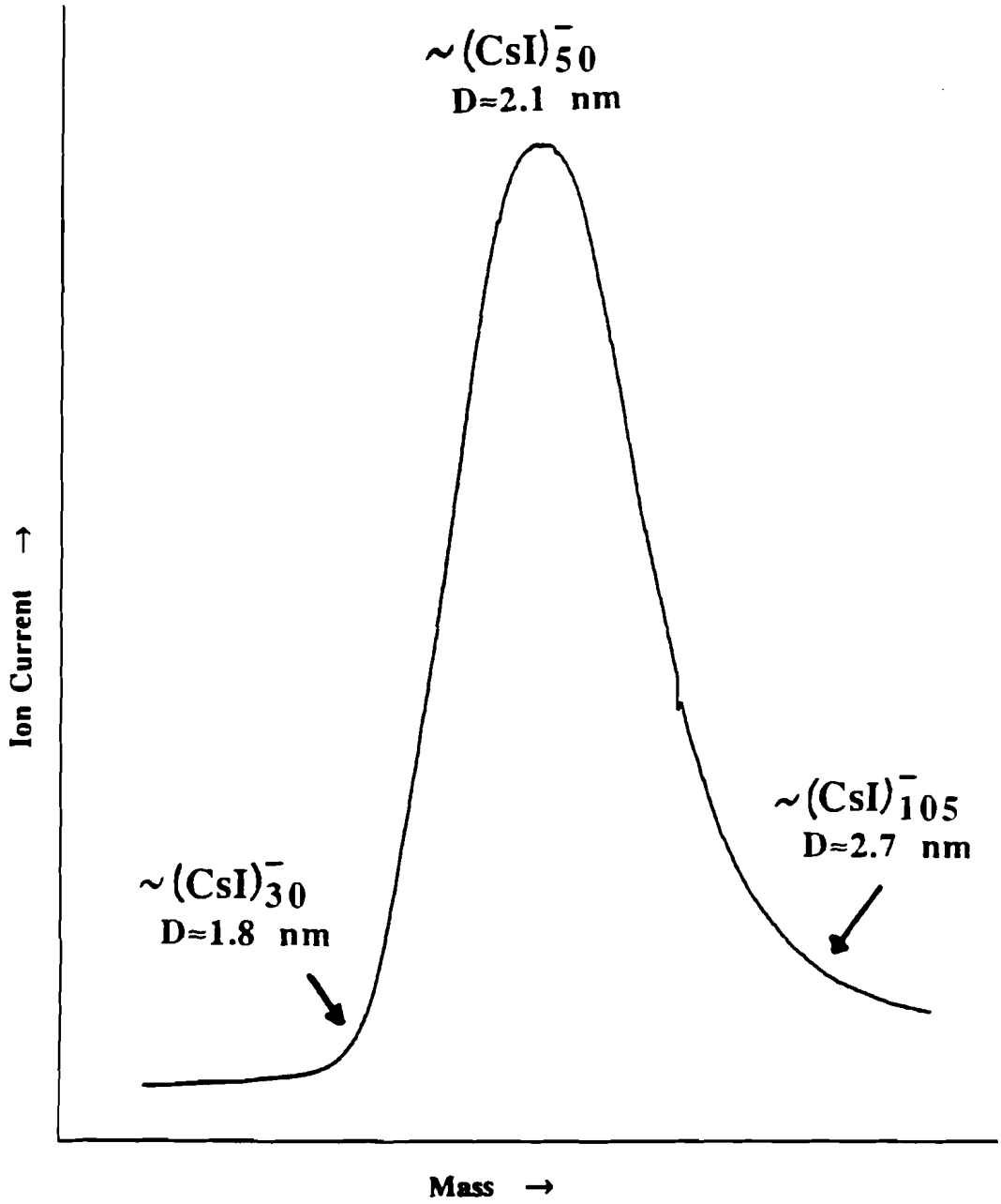

Figure 8: Mass Spectrum of Cesium Iodide Cluster Anions

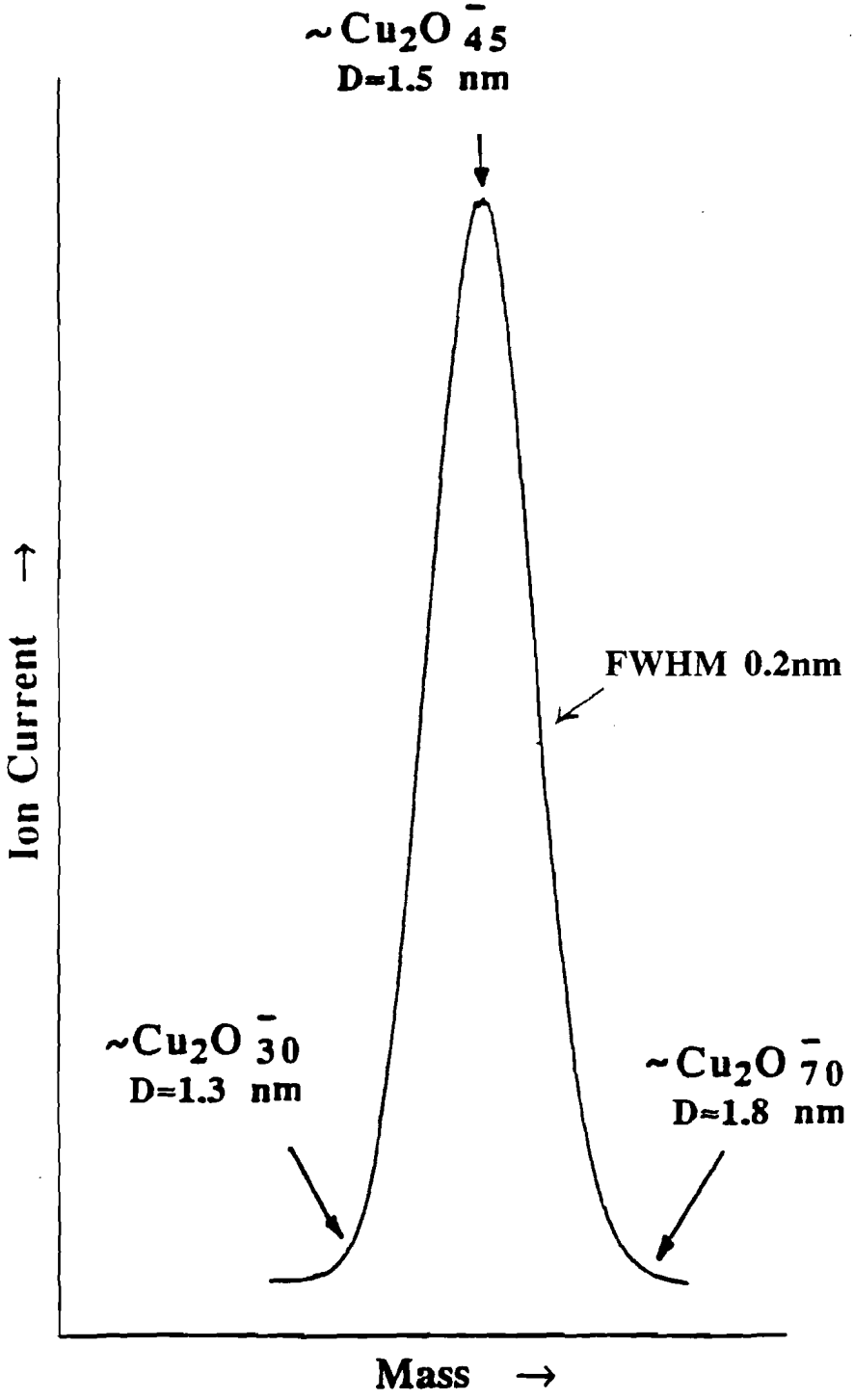

Figure 9: Mass Spectrum of Copper Oxide Cluster Anions

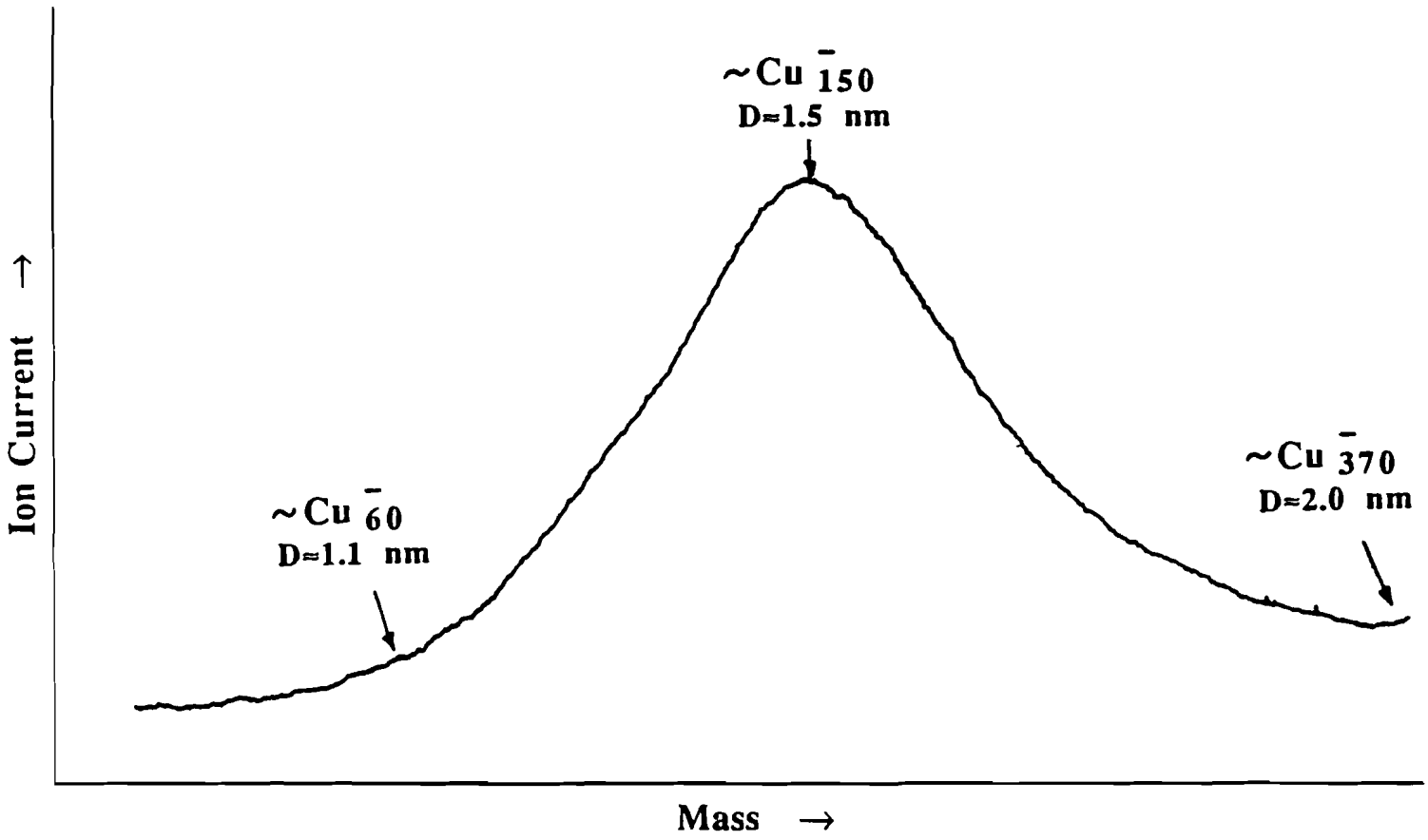

Figure 10: Mass Spectrum of Copper Cluster Anions

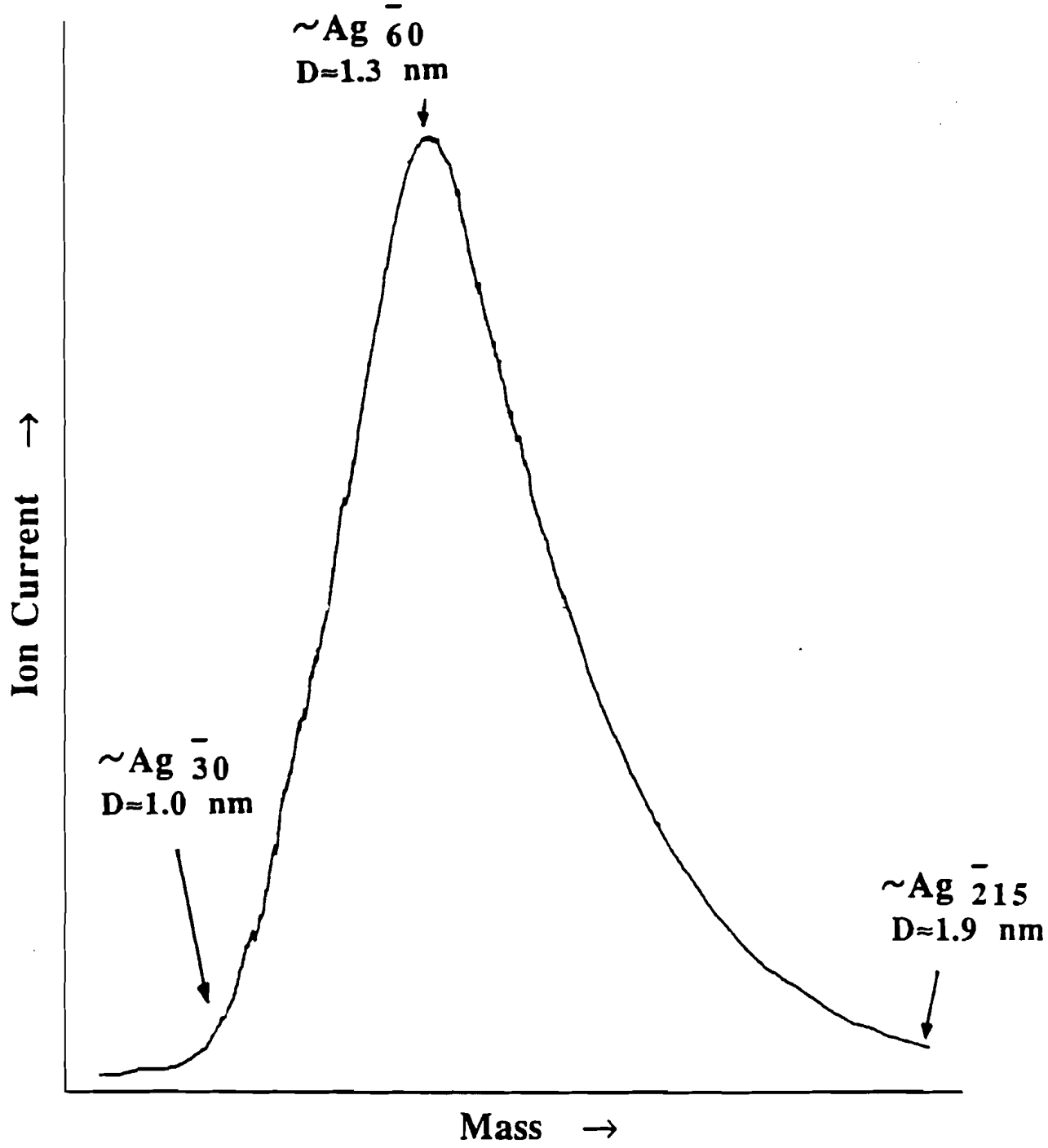

Figure 11: Mass Spectrum of Silver Cluster Anions

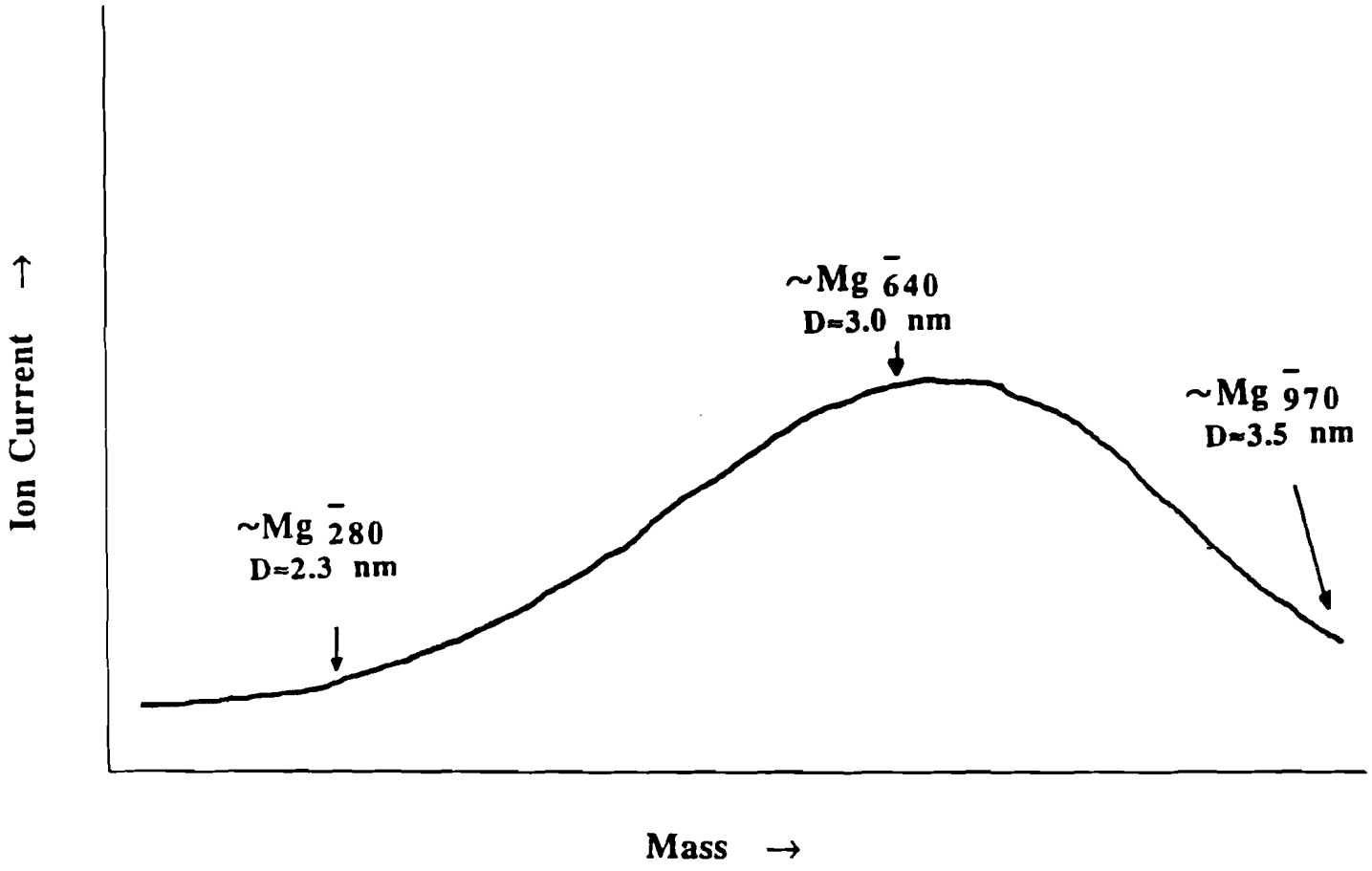

Figure 12: Mass Spectrum of Magnesium Cluster Anions

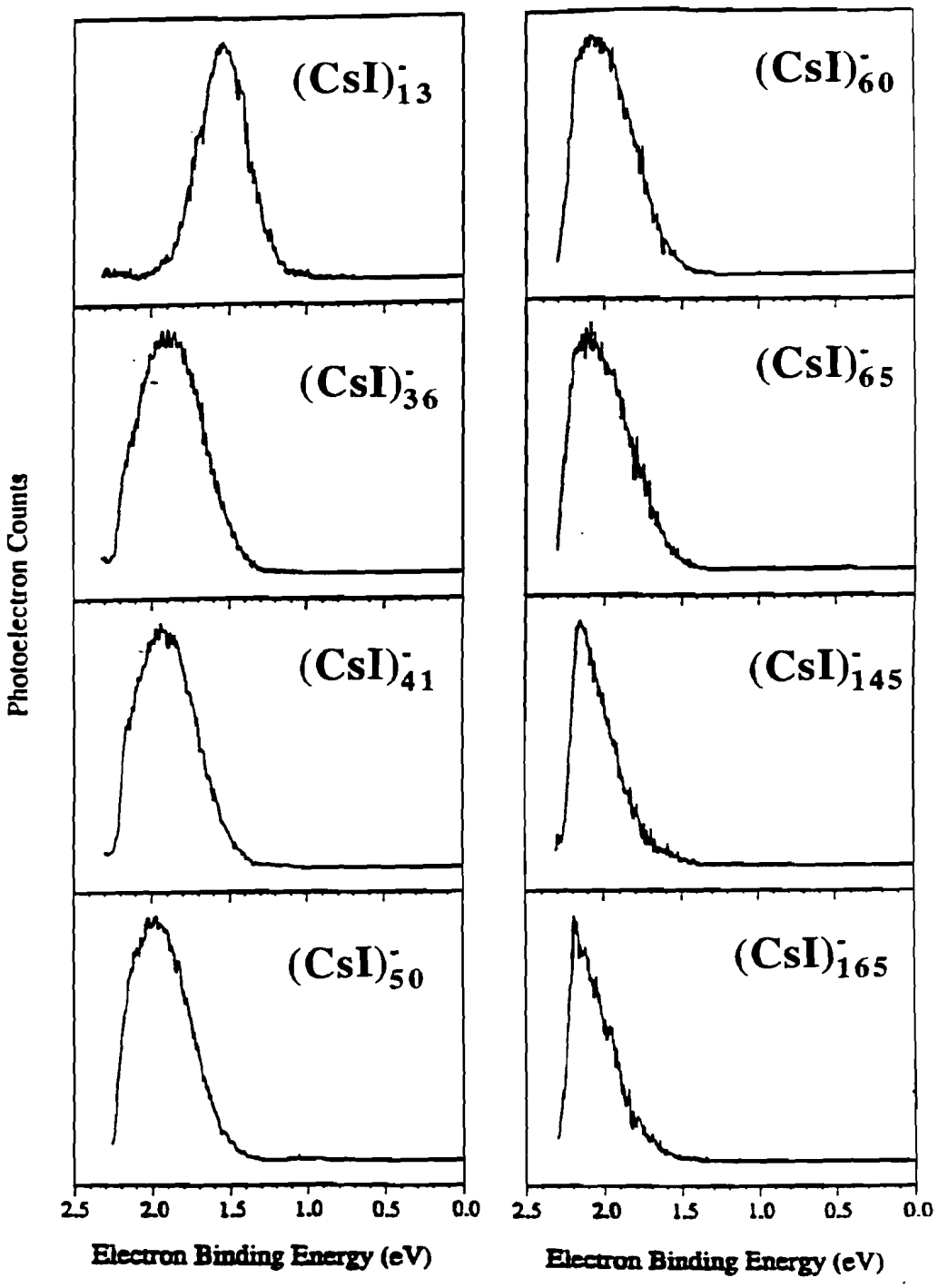

Figure 13: Photoelectron Spectra of Cesium Iodide Nanocluster Anions

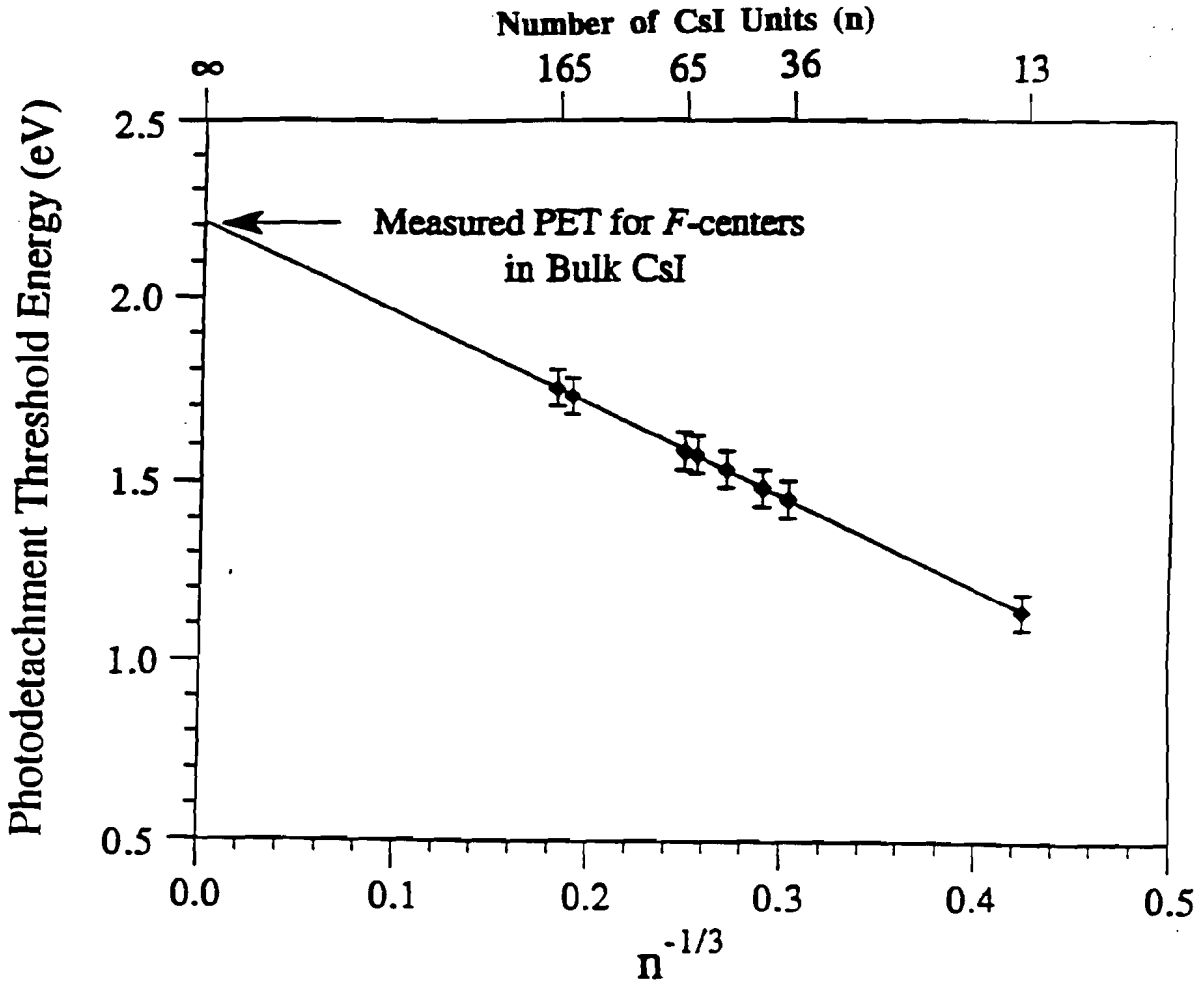

Figure 14: CsI Nanocrystal Anion Photodetachment Threshold Values vs. $n^{-1/3}$

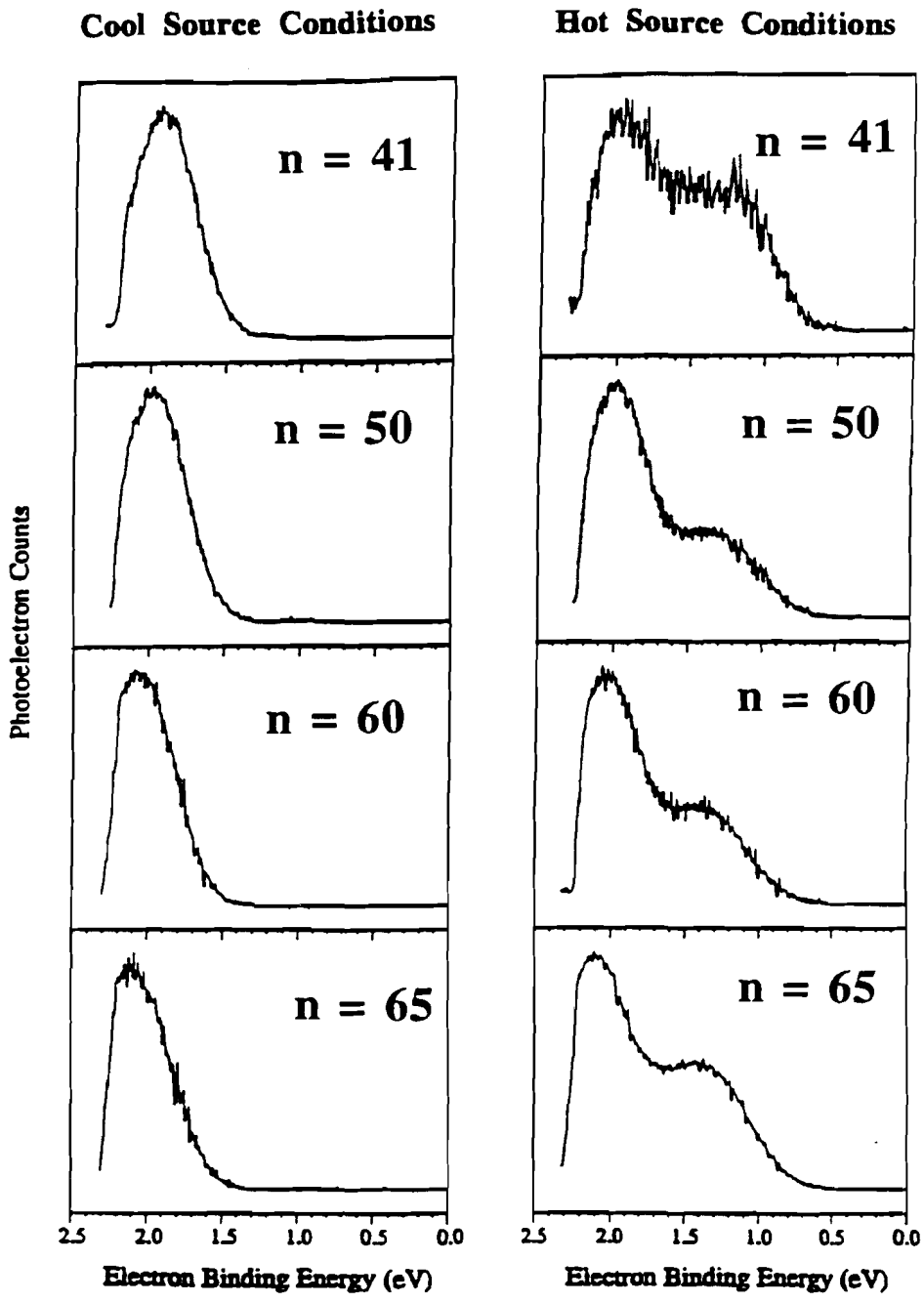

Figure 15: Photoelectron Spectra of CsI Nanocluster Anions Taken Under Different Source Conditions

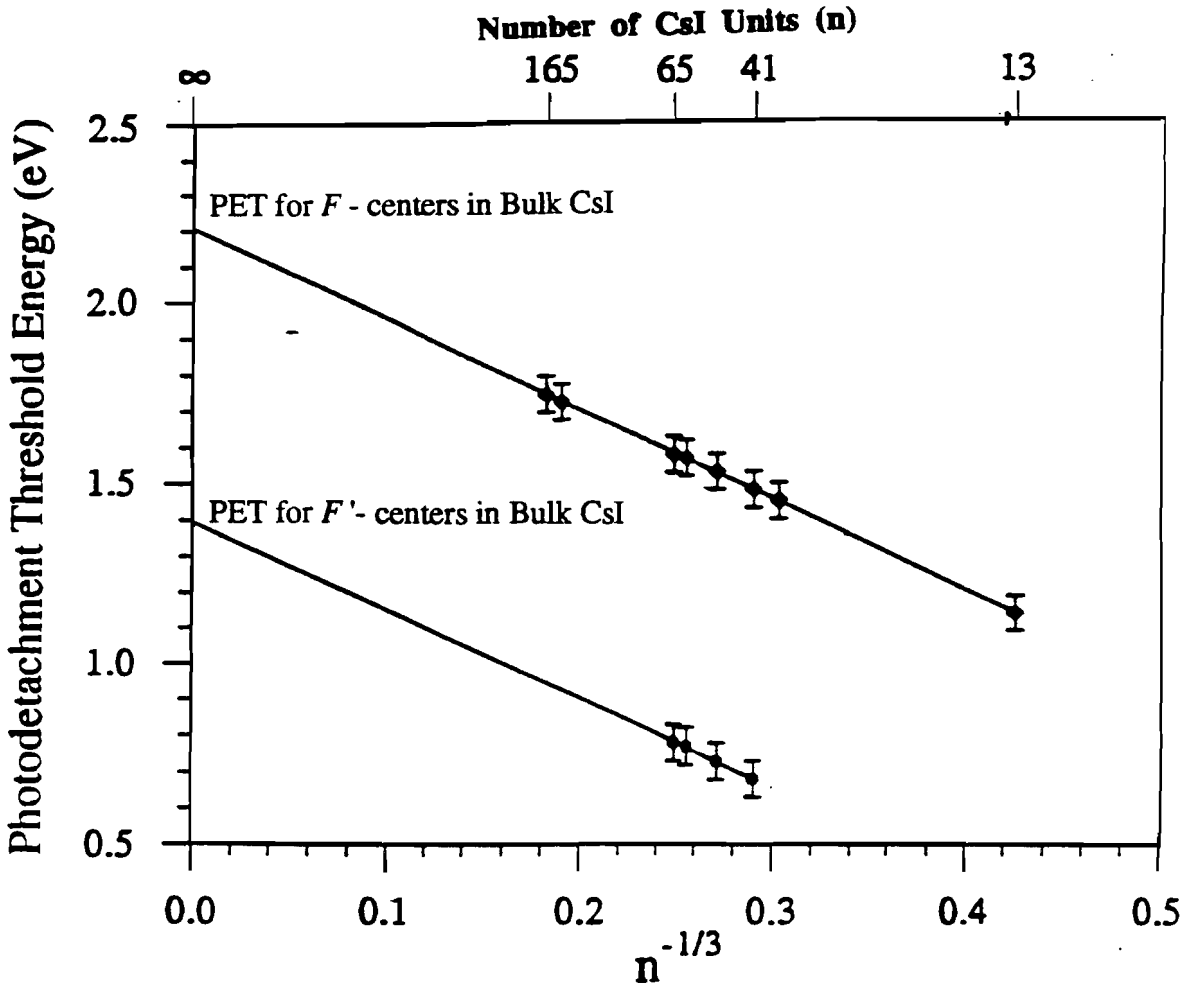

Figure 16: CsI Nanocrystal Anion Photodetachment Threshold Values vs. $n^{-1/3}$